

**Discrete breathers in a triangular  $\beta$ -Fermi-Pasta-Ulam-Tsingou lattice**Rita I. Babicheva,<sup>1</sup> Alexander S. Semenov ,<sup>2</sup> Elvira G. Soboleva ,<sup>3</sup> Aleksey A. Kudreyko ,<sup>4</sup>  
Kun Zhou ,<sup>5,\*</sup> and Sergey V. Dmitriev ,<sup>6,7</sup><sup>1</sup>*School of Mechanical and Aerospace Engineering, Nanyang Technological University, 50 Nanyang Avenue, Singapore 639798, Singapore*<sup>2</sup>*Polytechnic Institute (Branch) in Mirny, North-Eastern Federal University, Tikhonova St. 5/1, 678170 Mirny, Sakha Republic (Yakutia), Russia*<sup>3</sup>*Yurga Institute of Technology (Branch), National Research Tomsk Polytechnic University, 652050 Yurga, Russia*<sup>4</sup>*Department of Medical Physics and Informatics, Bashkir State Medical University, Lenin St. 3, 450008 Ufa, Russia*<sup>5</sup>*Environmental Process Modelling Centre, Nanyang Environment & Water Research Institute, Nanyang Technological University, 1 Cleantech Loop, Singapore 637141, Singapore*<sup>6</sup>*Institute for Metals Superplasticity Problems of RAS, Khalturin St. 39, Ufa 450000, Russia*<sup>7</sup>*Institute of Molecule and Crystal Physics, Ufa Federal Research Centre of RAS, Oktyabrya Ave. 151, Ufa 450075, Russia*

(Received 7 January 2021; accepted 30 March 2021; published 3 May 2021)

A practical approach to the search for (quasi-) discrete breathers (DBs) in a triangular  $\beta$ -FPUT lattice (after Fermi, Pasta, Ulam, and Tsingou) is proposed. DBs are obtained by superimposing localizing functions on delocalized nonlinear vibrational modes (DNVMs) having frequencies above the phonon spectrum of the lattice. Zero-dimensional and one-dimensional DBs are obtained. The former ones are localized in both spatial dimensions, and the latter ones are only in one dimension. Among the one-dimensional DBs, two families are considered: the first is based on the DNVMs of a triangular lattice, and the second is based on the DNVMs of a chain. We speculate that our systematic approach on the triangular  $\beta$ -FPUT lattice reveals all possible types of spatially localized oscillations with frequencies bifurcating from the upper edge of the phonon band as all DNVMs with frequencies above the phonon band are analyzed.

DOI: [10.1103/PhysRevE.103.052202](https://doi.org/10.1103/PhysRevE.103.052202)**I. INTRODUCTION**

Discrete nonlinear lattices support spatially localized oscillations called discrete breathers (DBs) (or intrinsic localized modes) [1–6]. The existence of DBs has been proved experimentally in various periodic systems such as cantilever arrays [7–9], Josephson junction arrays [10,11], electrical lattices [12,13], mass-spring chains [14], arrays of coupled pendula [15], chains of magnetic pendulums [16], and granular crystals [17,18]. They also exist in crystals [6], for example, in ionic NaI [19–23], covalent Si, Ge, and diamond [24,25], in pure metals with fcc, bcc, and hcp lattices [26–32] and in  $\alpha$ -uranium [33,34], in ordered alloys [35–38], and in hydrocarbons [39–51] and *h*-BN [52], as well as in proteins [53–57].

In many classical works, the existence of DBs was proved as exact solutions in nonlinear chains (see [2,3] and reviews [4,5]). From the standpoint of mathematical physics, DBs are single-frequency periodic, spatially localized vibrational modes having an infinitely long lifetime in the absence of perturbations. For complex nonlinear lattices, for example, crystals, numerical methods are used to find spatially localized vibrational modes that can be classified as quasibreathers [58], as was introduced by Chechin *et al.* Quasibreathers generalize the DB concept by considering spatially localized modes that are not single-frequency modes and have a long

but limited lifetime. In this paper, only quasibreathers are considered and are called DBs for brevity.

Some DBs can propagate with very little energy emission [59–63], but this topic is not considered further in the present paper. DBs are effective phonon scatterers [64,65] and hence reduce the thermal conductivity [66,67]. They affect other macroscopic properties of nonlinear lattices and crystals [68], for instance, elastic constants [69], thermal expansion [69,70], and heat capacity [69,71,72]. They can also transport electric charge [73].

Triangular nonlinear lattices are widely used in various applications [27,28,74–87]. Two types of DBs, symmetric and asymmetric ones, have been reported in a triangular Morse lattice with an on-site harmonic potential in the work [88]. Two types of chaotic DBs have been observed in a two-dimensional Morse lattice with an on-site harmonic potential [89]. The existence and stability of three-site DBs in a scalar triangular lattice have been analyzed in [90,91]. Moving DBs were found in a scalar triangular FPUT lattice in [92]. An analytical description of transient thermal processes in the harmonic triangular lattice has been given in [93]. Moving DBs in two-dimensional lattice of different symmetry have been analyzed in [62,63].

Despite the importance of DBs in various branches of physics, there were no general methods for finding all possible types of DBs in a given lattice. In the present study, we attempt to describe all possible DBs in a triangular  $\beta$ -FPUT lattice (named after Fermi, Pasta, Ulam, and Tsingou). The DBs

\*Corresponding author: [kzhou@ntu.edu.sg](mailto:kzhou@ntu.edu.sg)

are found by imposing localizing functions on delocalized nonlinear vibrational modes (DNVMs) of the triangular lattice [94] and linear chain [95]. Note that DNVMs are spatially periodic and exact oscillatory solutions to nonlinear equations of particle motion. They are obtained by taking into account only the lattice symmetry and therefore exist for any type of interparticle interactions and for any amplitude [96–99]. In the theoretical works [96–99] DNVMs are called bushes of nonlinear normal modes (BNNMs).

The dynamics of an one-component DNVM is described by the single equation of motion, while the  $m$ -component DNVM is described by a set of  $m$  coupled equations of motion. Consequently, the one-component DNVM is time periodic, while the  $m$ -component DNVM is, generally speaking, aperiodic with  $m$  incommensurate basis frequencies. For particular relations between amplitudes of DNVM components, periodic motion can be achieved [94,100].

DNVMs (or BNNMs) have been analyzed in molecules [101], nonlinear lattices [95,102–104], and crystals [27–29,105,106]. DNVMs derived in the hexagonal lattice [107] were studied in graphene [50,100,108,109] and  $h$ -BN [52]. Several one-component DNVMs were used to excite DBs with spherical symmetry in bcc metals V and Nb [106]. In another work [95], one- and two-component DNVMs (BNNMs) in the Fermi-Pasta-Ulam chain were derived and analyzed. The one-component DNVMs were excited in the chain with the following periodic patterns of initial atomic displacements:  $[A, -A]$ ,  $[A, 0, -A]$ ,  $[A, 0, -A, 0]$ , and  $[A, A, -A, -A]$ , where  $A$  denotes the DNVM amplitude. Later, in [110], these modes were excited in a close-packed atomic row of a triangular Lennard-Jones lattice. The obtained vibrational modes were called one-dimensional DBs.

In the recent work by Watanabe and Izumi, exact DB solutions in a two-dimensional hexagonal Fermi-Pasta-Ulam lattice were obtained, and the relation of the DBs with DNVMs of the hexagonal lattice was demonstrated [111].

In the present work an attempt is made to describe all possible types of DBs in the  $\beta$ -FPUT triangular lattice. We have chosen the  $\beta$ -FPUT model because it is a classical model and recently all one- and two-component DNVMs for this lattice were derived [94]. Three of them have frequencies above the phonon spectrum, and they will be used to construct the DB solutions.

This paper is organized as follows. The model and simulation details are described in Sec. II. Analytical results for DNVMs of the triangular  $\beta$ -FPUT lattice are reported in Sec. III. The properties of DNVMs of the triangular lattice are presented in Sec. IV. Examples of DBs based on DNVMs of the triangular lattice are given in Sec. V. DBs based on DNVMs of a chain are described in Sec. VI. The results are discussed and summarized in Sec. VII.

## II. MODEL AND SIMULATION SETUP

A two-dimensional triangular lattice of particles having mass  $m$  and interacting with the nearest neighbors is considered on the  $x$ - $y$  plane; see Fig. 1. The distance between the nearest lattice points is equal to  $h$ . The primitive translational cell of the lattice has vectors of translation  $(h, 0)$  and  $(h/2, h\sqrt{3}/2)$ . The simulation box has  $N_x \times N_y$  prim-

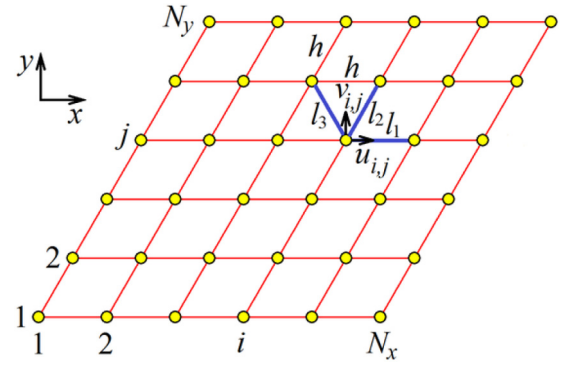


FIG. 1. Computational cell for the triangular lattice with the lattice spacing  $h$  including  $N_x \times N_y$  particles numbered by indices  $i = 1, 2, \dots, N_x$  and  $j = 1, 2, \dots, N_y$ . Particles in their equilibrium positions are shown by yellow circles, and red lines show the primitive translational cells. The particles moving in the  $x$ - $y$  plane have two degrees of freedom, the components of the displacement vector  $(u_{i,j}, v_{i,j})$ . Each particle interacts with its six nearest neighbors via the  $\beta$ -FPUT potential (3). The bonds are shown only for one translational cell of the lattice; they are designated as  $l_1, l_2$ , and  $l_3$ .

itive translational cells (or particles), and the values  $N_x$  and  $N_y$  are given below for each particular problem. Particles are numbered by the indices  $i = 1, 2, \dots, N_x$  and  $j = 1, 2, \dots, N_y$ . Each particle moving in the  $xy$ -plane has two degrees of freedom, the components of the displacement vector  $(u_{i,j}(t), v_{i,j}(t))$ , which are unknown functions of time  $t$ . The components of the particle velocity vector are  $(\dot{u}_{i,j}, \dot{v}_{i,j})$ , where the overdot means differentiation with respect to time.

Referring to Fig. 1, one can write expressions for the lengths of six bonds,  $l_1, l_2, \dots$ , and  $l_6$ , connecting the  $i, j$ th particle with its nearest neighbors,

$$\begin{aligned} l_1^2 &= (h + u_{i+1,j} - u_{i,j})^2 + (v_{i+1,j} - v_{i,j})^2, \\ l_2^2 &= \left(\frac{h}{2} + u_{i,j+1} - u_{i,j}\right)^2 + \left(\frac{h\sqrt{3}}{2} + v_{i,j+1} - v_{i,j}\right)^2, \\ l_3^2 &= \left(-\frac{h}{2} + u_{i-1,j+1} - u_{i,j}\right)^2 + \left(\frac{h\sqrt{3}}{2} + v_{i-1,j+1} - v_{i,j}\right)^2, \\ l_4^2 &= (-h + u_{i-1,j} - u_{i,j})^2 + (v_{i-1,j} - v_{i,j})^2, \\ l_5^2 &= \left(-\frac{h}{2} + u_{i,j-1} - u_{i,j}\right)^2 + \left(-\frac{h\sqrt{3}}{2} + v_{i,j-1} - v_{i,j}\right)^2, \\ l_6^2 &= \left(\frac{h}{2} + u_{i+1,j-1} - u_{i,j}\right)^2 + \left(-\frac{h\sqrt{3}}{2} + v_{i+1,j-1} - v_{i,j}\right)^2. \end{aligned} \quad (1)$$

The Hamiltonian of the model is

$$\begin{aligned} H &= \frac{m}{2} \sum_{i,j} (\dot{u}_{i,j}^2 + \dot{v}_{i,j}^2) + \sum_{i,j} [\varphi(l_1 - h) \\ &\quad + \varphi(l_2 - h) + \varphi(l_3 - h)], \end{aligned} \quad (2)$$

where the first (second) sum gives the kinetic (potential) energy of the simulation box and  $l_1, l_2$ , and  $l_3$  are the bond lengths for the three bonds in the  $i, j$ th primitive translational cell, as given by Eq. (1).

The energy of the bond connecting the two nearest particles is described by the  $\beta$ -FPUT potential

$$\varphi(r) = \frac{k}{2}(r-h)^2 + \frac{\beta}{4}(r-h)^4, \quad (3)$$

where  $r$  is the distance between the particles,  $k$  is the linear stiffness of the bond, and  $\beta$  is the nonlinearity coefficient. We set  $h = 1$ ,  $k = 1$  (for dimensional homogeneity), and  $\beta = 10$ . With this value of  $\beta$ , all the effects of nonlinearity become

pronounced for particle displacements of the order of 0.1, as in typical crystal lattices. Indeed, we obtain DBs with the amplitude of the order of 0.1, when the linear term is of order of 0.01 and the contribution from the quartic term is about 0.001. Therefore, the contribution from the nonlinear term is about 10%, which is not negligible. The mass of the particles, as mentioned above, is set equal to 1, and this can always be achieved by choosing a unit of time.

Using Hamilton's equations, the following equations of motion can be derived from the Hamiltonian (2):

$$\begin{aligned} m\ddot{u}_{i,j} &= (h + u_{i+1,j} - u_{i,j})[k(l_1 - h) + \beta(l_1 - h)^3]/l_1 + \left(\frac{h}{2} + u_{i,j+1} - u_{i,j}\right)[k(l_2 - h) + \beta(l_2 - h)^3]/l_2 \\ &+ \left(-\frac{h}{2} + u_{i-1,j+1} - u_{i,j}\right)[k(l_3 - h) + \beta(l_3 - h)^3]/l_3 + (-h + u_{i-1,j} - u_{i,j})[k(l_4 - h) + \beta(l_4 - h)^3]/l_4 \\ &+ \left(-\frac{h}{2} + u_{i,j-1} - u_{i,j}\right)[k(l_5 - h) + \beta(l_5 - h)^3]/l_5 + \left(\frac{h}{2} + u_{i+1,j-1} - u_{i,j}\right)[k(l_6 - h) + \beta(l_6 - h)^3]/l_6, \quad (4) \\ m\ddot{v}_{i,j} &= (v_{i+1,j} - v_{i,j})[k(l_1 - h) + \beta(l_1 - h)^3]/l_1 + \left(\frac{h\sqrt{3}}{2} + v_{i,j+1} - v_{i,j}\right)[k(l_2 - h) + \beta(l_2 - h)^3]/l_2 \\ &+ \left(\frac{h\sqrt{3}}{2} + v_{i-1,j+1} - v_{i,j}\right)[k(l_3 - h) + \beta(l_3 - h)^3]/l_3 + (v_{i-1,j} - v_{i,j})[k(l_4 - h) + \beta(l_4 - h)^3]/l_4 \\ &+ \left(-\frac{h\sqrt{3}}{2} + v_{i,j-1} - v_{i,j}\right)[k(l_5 - h) + \beta(l_5 - h)^3]/l_5 + \left(-\frac{h\sqrt{3}}{2} + v_{i+1,j-1} - v_{i,j}\right)[k(l_6 - h) + \beta(l_6 - h)^3]/l_6. \quad (5) \end{aligned}$$

Linearized equations of motion are

$$\begin{aligned} m\ddot{u}_{i,j} &= k(u_{i-1,j} - 2u_{i,j} + u_{i+1,j}) + \frac{k}{4}[u_{i,j+1} - u_{i,j} + \sqrt{3}(v_{i,j+1} - v_{i,j})] + \frac{k}{4}[u_{i-1,j+1} - u_{i,j} - \sqrt{3}(v_{i-1,j+1} - v_{i,j})] \\ &+ \frac{k}{4}[u_{i,j-1} - u_{i,j} + \sqrt{3}(v_{i,j-1} - v_{i,j})] + \frac{k}{4}[u_{i+1,j-1} - u_{i,j} - \sqrt{3}(v_{i+1,j-1} - v_{i,j})], \quad (6) \end{aligned}$$

$$\begin{aligned} m\ddot{v}_{i,j} &= \frac{k\sqrt{3}}{4}[u_{i,j+1} - u_{i,j} + \sqrt{3}(v_{i,j+1} - v_{i,j})] - \frac{k\sqrt{3}}{4}[u_{i-1,j+1} - u_{i,j} - \sqrt{3}(v_{i-1,j+1} - v_{i,j})] \\ &+ \frac{k\sqrt{3}}{4}[u_{i,j-1} - u_{i,j} + \sqrt{3}(v_{i,j-1} - v_{i,j})] - \frac{k\sqrt{3}}{4}[u_{i+1,j-1} - u_{i,j} - \sqrt{3}(v_{i+1,j-1} - v_{i,j})]. \quad (7) \end{aligned}$$

Looking for the solution of Eqs. (6) and (7) in the form  $u_{i,j} = F \exp[\mathbf{i}(qi + pj - \omega t)]$ ,  $v_{i,j} = B \exp[\mathbf{i}(qi + pj - \omega t)]$ , where  $\mathbf{i}$  is imaginary unit, one finds the dispersion relation

$$\omega_{1,2}^2(q, p) = \frac{-\xi \pm \sqrt{\xi^2 - 4\alpha\gamma}}{2\alpha}, \quad (8)$$

where

$$\begin{aligned} \alpha &= 4m^2, \\ \xi &= 8mk(S + \cos q - 1), \\ \gamma &= 3k^2[4(\cos q - 1)S + S^2 - Q^2], \\ S &= \cos p + \cos(q - p) - 2, \\ Q &= \cos p - \cos(q - p). \quad (9) \end{aligned}$$

For further discussion the highest phonon frequency is important. For the model parameters used in this study

( $k = m = 1$ ), the maximum frequency  $\omega_{\max} = \sqrt{6}$  is observed at eight points of the first Brillouin zone,  $(q, p) = (\pm\pi, \pm\pi)$ ,  $(q, p) = (\pm\pi, 0)$ , and  $(q, p) = (0, \pm\pi)$ .

Periodic boundary conditions are taken in both directions in the study of DNVMs. In the study of DBs, absorbing boundary conditions are used, which remove radiation emitted at an early stage of DB evolution.

The time step for these simulations is taken to be 0.002 time units with the use of the symplectic Störmer integrator of order six [112].

Initial conditions are set by applying initial displacements to the particles as described below. Initial velocities of all particles are always equal to zero. Since all particles have zero initial velocity, the total momentum transferred to the lattice is zero. More details on the excitation of one- and two-component DNVMs are provided later.

### III. ANALYTICAL RESULTS

Since our approach to finding new types of quasi-DBs is based on the imposition of localizing functions on DNVMs with frequencies outside the phonon spectrum, it is important to show that the DNVMs studied in this work have frequencies above the phonon spectrum. According to our previous work [94], there are three such DNVMs: the one-component DNVMs 2 and 4 and the time-periodic two-component DNVM  $\gamma 2$ ; see Figs. 2(a)–2(c), respectively. In our previous work [94] this was demonstrated numerically, but here

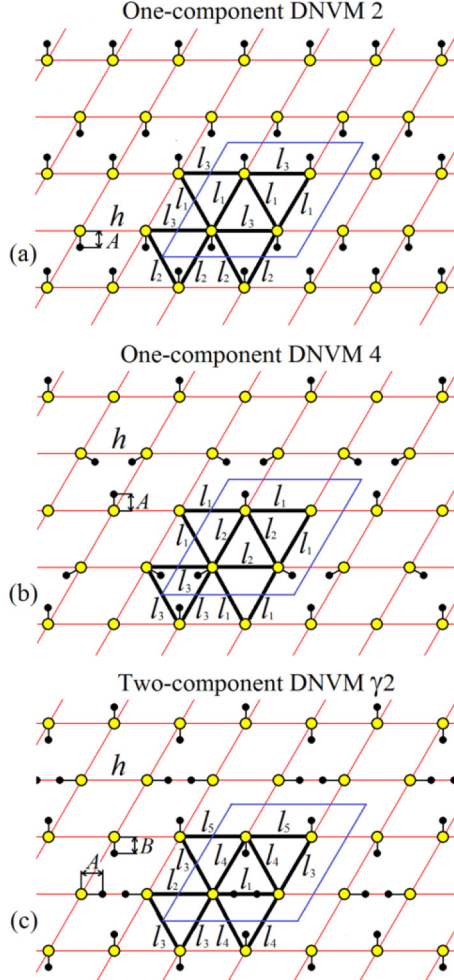


FIG. 2. Three DNVMs of the triangular lattice considered in this study: (a) one-component DNVM 2, (b) one-component DNVM 4, and (c) two-component time-periodic DNVM  $\gamma 2$  [94]. The distance between nearest particles is  $h$ . Particles in the equilibrium positions are shown by the yellow circles. Red lines show the primitive translational cells of the lattice. Translational cells of DNVMs include four particles and are shown by the blue lines. The bonds are shown only for one translational cell of the DNVM; they are designated as  $l_k$ . The black dots show the initial particle displacements used to excite the DNVMs. In (a) and (b), all displacement vectors have a length  $A$ , while in (c), horizontal and vertical displacements have magnitudes  $A$  and  $B$ , respectively. In (a) and (c), all particles are displaced at  $t = 0$ ; in (b), one of the four particles in the translational cell is not displaced initially and remains at rest at any  $t$ . Each translational cell includes 12 bonds shown by the solid black lines. The bonds have lengths  $l_i$ .

we confirm the numerical results with analytics. The DNVM notation does not reflect any physical meaning, it simply coincides with that used in [94].

For the two-component DNVM  $\gamma 2$ , it is also very important to find the relationship between the two components, resulting in a time-periodic dynamic. This is necessary because DBs are single-frequency localized modes and single-frequency DNVMs should be used to excite them, while two-component DNVMs are, generally speaking, a mixture of two modes with incommensurate frequencies.

In Fig. 2 the particles in equilibrium positions are shown by yellow circles, and the black dots show the initial positions of particles used for the excitation of these modes with zero initial velocities. The red lines show the primitive translational cells of the lattice. In Figs. 2(a) and 2(b) all initial displacement vectors have the same length  $A$ . In Fig. 2(c) horizontal (vertical) initial displacement vectors have a length  $A$  ( $B$ ). If  $A$  and  $B$  are properly chosen, the two-component DNVM  $\gamma 2$  exhibits periodic motion with respect to time [94].

The Hamiltonian and equations of motion for each of the DNVMs shown in Fig. 2 are presented below.

#### A. One-component DNVM 2

We begin with the one-component DNVM 2, where all nodes in lattice are in motion, and all nodes in the same row move identically, as shown in Fig. 2(a). By taking into account the symmetry of the mode, it is possible to write down the Hamiltonian of the one-component DNVM 2,

$$H = \frac{m\dot{a}^2}{2} + \varphi(l_1 - h) + \varphi(l_2 - h) + \varphi(l_3 - h), \quad (10)$$

where

$$l_1 = \sqrt{\left(\frac{h}{2}\right)^2 + \left(\frac{h\sqrt{3}}{2} + 2a\right)^2},$$

$$l_2 = \sqrt{\left(\frac{h}{2}\right)^2 + \left(\frac{h\sqrt{3}}{2} - 2a\right)^2}, \quad \text{and}$$

$$l_3 = h.$$

Parameter  $a(t)$  is the vertical displacement of any particle from its lattice position, and  $l_i$  ( $i = 1, 2$ , or  $3$ ) are the distances between nearest lattice points; see Fig. 2(a).

The equation of motion corresponding to the Hamiltonian in Eq. (10) has the form

$$m\ddot{a} = -\frac{h\sqrt{3} + 4a}{l_1}[k(l_1 - h) + \beta(l_1 - h)^3] + \frac{h\sqrt{3} - 4a}{l_2}[k(l_2 - h) + \beta(l_2 - h)^3]. \quad (11)$$

The expansion of the Hamiltonian in Eq. (10) up to quartic terms gives

$$H = \frac{m\dot{a}^2}{2} + 3ka^2 + \left(\frac{9\beta}{2} - \frac{11k}{4h^2}\right)a^4, \quad (12)$$

which can be used to derive the following cubic equation of motion:

$$m\ddot{a} = -6ka - \left(18\beta - \frac{11k}{h^2}\right)a^3. \quad (13)$$

The solution is in the form of  $a(t) = A_1 \sin(\omega t) + A_2 \sin(3\omega t)$ . By assuming that  $A_1 \ll h$  and  $A_2 \ll A_1$ , the frequency-amplitude relation can be found as follows:

$$\omega = \sqrt{\frac{6k}{m} + \frac{3}{8\sqrt{6km}} \left(18\beta - \frac{11k}{h^2}\right) A_1^2}. \quad (14)$$

When model parameters  $m = h = k = 1$  and  $\beta = 10$ , Eq. (14) is reduced to

$$\omega = \sqrt{6} + 25.87A_1^2. \quad (15)$$

As mentioned above, the upper edge of the phonon band of the considered lattice is

$$\omega_{\max} = \sqrt{6} \approx 2.449, \quad (16)$$

and thus, the frequency of the DNVM 2 is above the phonon band.

The obtained solution (14) assumes small displacements, while the exact solution can be expressed in terms of the elliptic functions.

### B. One-component DNVM 4

The Hamiltonian of the one-component DNVM 4 is

$$H = \frac{3}{4} \frac{m\dot{a}^2}{2} + \frac{3}{2} \varphi(l_1 - h) + \frac{3}{4} [\varphi(l_2 - h) + \varphi(l_3 - h)], \quad (17)$$

where

$$\begin{aligned} l_1 &= \sqrt{h^2 + a^2}, \\ l_2 &= h + a\sqrt{3}, \quad \text{and} \\ l_3 &= h - a\sqrt{3}. \end{aligned}$$

Similar to the one-component DNVM 2 case,  $a(t)$  is the displacement of a moving particle from its lattice position and  $l_i$  ( $i = 1, 2$ , or  $3$ ) is the distance between nearest lattice points; see Fig. 2(b). Since only three of the four particles in the translational cell are in motion, the effective mass in the Hamiltonian is equal to  $3m/4$ .

The equation of motion corresponding to the Hamiltonian (17) is

$$\begin{aligned} \frac{3}{4} m\ddot{a} &= -\frac{3a}{2l_1} [k(l_1 - h) + \beta(l_1 - h)^3] \\ &\quad - \frac{3\sqrt{3}}{4} [k(l_2 - h) + \beta(l_2 - h)^3] \\ &\quad + \frac{3\sqrt{3}}{4} [k(l_3 - h) + \beta(l_3 - h)^3]. \end{aligned} \quad (18)$$

Expansion of the Hamiltonian (17) up to quartic terms has the form

$$H = \frac{3}{4} \frac{m\dot{a}^2}{2} + \frac{9}{4} ka^2 + \left(\frac{3k}{16h^2} + \frac{27\beta}{8}\right)a^4. \quad (19)$$

The cubic equation of motion stemming from Eq. (19) is

$$m\ddot{a} = -6ka - \left(\frac{k}{h^2} + 18\beta\right)a^3. \quad (20)$$

The solution is in the form of  $a(t) = A_1 \sin(\omega t) + A_2 \sin(3\omega t)$ . By assuming that  $A_1 \ll h$  and  $A_2 \ll A_1$ , the frequency-amplitude relation can be found as follows:

$$\omega = \sqrt{\frac{6k}{m} + \frac{3}{8\sqrt{6km}} \left(\frac{k}{h^2} + 18\beta\right) A_1^2}. \quad (21)$$

When  $m = h = k = 1$  and  $\beta = 10$ , Eq. (21) can be reduced to

$$\omega = \sqrt{6} + 27.71A_1^2. \quad (22)$$

This mode also has frequencies above the upper phonon band edge  $\omega_{\max} = \sqrt{6}$ .

Instead of the approximate solution (21) the exact solution can be given in terms of the elliptic functions.

### C. Time periodic two-component DNVM $\gamma 2$

The Hamiltonian of the two-component time-periodic DNVM  $\gamma 2$  is

$$\begin{aligned} H &= \frac{m}{4} (\dot{a}^2 + \dot{b}^2) + \frac{1}{4} \varphi(l_1 - h) + \frac{1}{4} \varphi(l_2 - h) \\ &\quad + \varphi(l_3 - h) + \varphi(l_4 - h) + \frac{1}{2} \varphi(l_5 - h), \end{aligned} \quad (23)$$

where

$$\begin{aligned} l_1 &= h - 2a, \\ l_2 &= h + 2a, \\ l_3 &= \sqrt{\left(\frac{h}{2} + a\right)^2 + \left(\frac{h\sqrt{3}}{2} + b\right)^2}, \\ l_4 &= \sqrt{\left(\frac{h}{2} - a\right)^2 + \left(\frac{h\sqrt{3}}{2} - b\right)^2}, \quad \text{and} \\ l_5 &= \sqrt{h^2 + (2b)^2}. \end{aligned}$$

Parameters  $a(t)$  and  $b(t)$  are the horizontal and vertical displacements of the particles from their lattice positions, respectively and  $l_i$  ( $i = 1, 2, \dots$ , or  $5$ ) is the distance between nearest lattice points; see Fig. 2(c). The effective mass is equal to  $m/2$  because this mode is a superposition of two modes, in each of which only half of the particles move [94].

The equations of motion corresponding to the Hamiltonian in Eq. (23) have the form

$$\begin{aligned} \frac{m}{2} \ddot{a} &= \frac{1}{2} [k(l_1 - h) + \beta(l_1 - h)^3] \\ &\quad - \frac{1}{2} [k(l_2 - h) + \beta(l_2 - h)^3] \\ &\quad + \frac{h - 2a}{2l_3} [k(l_3 - h) + \beta(l_3 - h)^3] \\ &\quad - \frac{(h + 2a)}{2l_4} [k(l_4 - h) + \beta(l_4 - h)^3] \quad \text{and} \quad (24) \\ \frac{m}{2} \ddot{b} &= \frac{\sqrt{3}h - 2b}{2l_3} [k(l_3 - h) + \beta(l_3 - h)^3] \end{aligned}$$

$$\begin{aligned}
 & - \frac{\sqrt{3}h + 2b}{2l_4} [k(l_4 - h) + \beta(l_4 - h)^3] \\
 & - \frac{b}{l_5} [k(l_5 - h) + \beta(l_5 - h)^3]. \quad (25)
 \end{aligned}$$

The expansion of the Hamiltonian (23) up to quartic terms gives

$$\begin{aligned}
 H = & \frac{m}{4}(\dot{a}^2 + \dot{b}^2) + ka^2 + \frac{k}{4}(a + \sqrt{3}b)^2 + \frac{k}{h^2}b^4 + 2\beta a^4 \\
 & + \frac{\beta}{32}(a + \sqrt{3}b)^4 - \frac{k}{64h^2}(3a^4 - 26a^2b^2 + 11b^4 \\
 & - 12\sqrt{3}ab^3 + 28\sqrt{3}a^3b). \quad (26)
 \end{aligned}$$

The cubic equations of motion corresponding to the Hamiltonian in Eq. (26) are

$$\begin{aligned}
 m\ddot{a} = & -5ka - \sqrt{3}kb - 16\beta a^3 - \frac{\beta}{4}(a + \sqrt{3}b)^3 \\
 & + \frac{k}{8h^2}(3a^3 + 21\sqrt{3}a^2b - 13ab^2 - 3\sqrt{3}b^3) \quad \text{and} \quad (27) \\
 m\ddot{b} = & -\sqrt{3}ka - 3kb - \frac{8}{h^2}kb^3 - \frac{\beta\sqrt{3}}{4}(a + \sqrt{3}b)^3 \\
 & + \frac{k}{8h^2}(7\sqrt{3}a^3 - 13a^2b - 9\sqrt{3}ab^2 + 11b^3). \quad (28)
 \end{aligned}$$

The relation between the DNVM components  $a$  and  $b$  is to be found when the linearized equations of motion (27) and (28) have a time-periodic solution. The following expression is substituted into these equations:

$$a = pb, \quad (29)$$

where  $p$  is the unknown constant. The results read

$$m\ddot{a} = -\omega_a^2 a \quad \text{and} \quad m\ddot{b} = -\omega_b^2 b, \quad (30)$$

where  $\omega_a^2 = (5 + \sqrt{3}/p)k$  and  $\omega_b^2 = (3 + \sqrt{3}p)k$ . The small-amplitude vibration frequencies  $\omega_a$  and  $\omega_b$  are equal if  $p = (1 \pm 2)/\sqrt{3}$ . The root with a negative sign produces the mode with frequency equal to  $\omega_a = \omega_b = \sqrt{2k}$  (time-periodic DNVM  $\gamma 1$ ; see [94]), which is within the phonon spectrum. The root with a positive sign, i.e.,  $p = \sqrt{3}$  is analyzed. It produces the mode with the frequency  $\omega_a = \omega_b = \sqrt{6k}$  (time-periodic DNVM  $\gamma 2$ ; see [94]), which is at the upper edge of the phonon band.

At small amplitudes  $A$  and  $B$ ,  $p = \sqrt{3}$ . The amplitudes are hence synchronized, and time-periodic motion is generated. When the amplitudes are large,  $p$  is no longer a constant but a function of  $A$ . Equation (29) therefore becomes

$$A = p(A)B. \quad (31)$$

Figure 3 shows the numerical dependence of  $p$  on  $A$ , where the DNVM  $\gamma 2$  becomes time periodic. The inset shows the coefficients of the polynomial approximation by the method of least squares.

#### IV. PROPERTIES OF DNVMs

Some properties of the three studied DNVMs of the triangular lattice are presented in Fig. 4. Black solid dots, red open

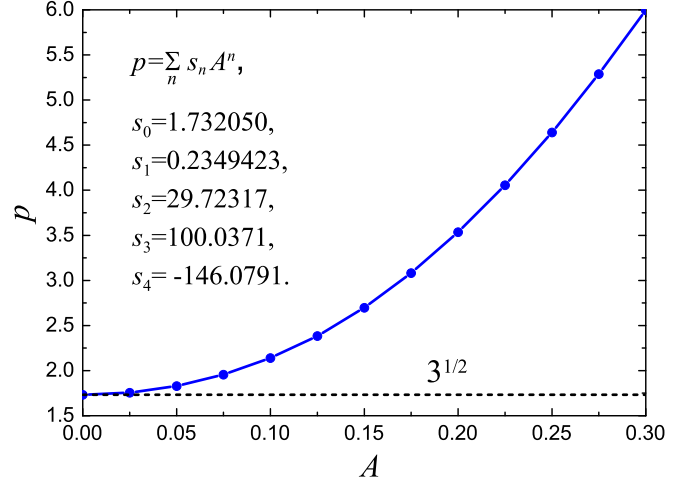


FIG. 3. Dependence of  $p$  on  $A$  in Eq. (31) when the two-component DNVM  $\gamma 2$  becomes time periodic. The inset shows the coefficients of the polynomial approximation by the method of least squares. The horizontal dashed line shows the synchronized conditions with  $p = \sqrt{3}$  for small  $A$ .

circles, and blue squares denote the DNVM 2, DNVM 4, and DNVM  $\gamma 2$ , respectively. For the two-component DNVM  $\gamma 2$ , Eq. (31) and Fig. 3 are used to calculate the amplitude  $B$  at the chosen amplitude  $A$ . The computational cell includes  $N_x \times N_y = 4 \times 4$  particles. Initial displacements of particles are set according to Fig. 2. Initial velocities of the particles are set equal to zero.

Figure 4(a) shows the frequency-amplitude dependencies for the DNVMs. The upper edge of the phonon band shown by the horizontal dashed line indicates that all the three DNVMs have frequencies above the phonon spectrum. As shown in Fig. 4(b), the energy per particle increases with the DNVM amplitude as  $E \sim A^2$ .

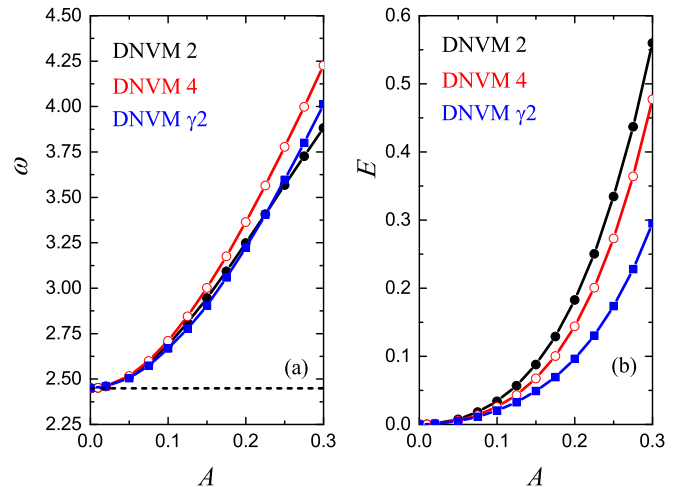


FIG. 4. (a) Frequency  $\omega$  and (b) energy per particle  $E$  as functions of amplitudes of the DNVM 2 (black solid dots), DNVM 4 (red open dots), and DNVM  $\gamma 2$  (blue squares). The horizontal dashed line in (a) indicates the upper edge of the phonon band with  $\omega_{\max} = \sqrt{6} \approx 2.449$  [94].

## V. DISCRETE BREATHERS

DBs are obtained by imposing localizing functions on the three DNVMs of the triangular lattice described in Sec. IV. The parameters of the localizing functions are selected by trial and error so as to obtain a localized vibrational mode with the maximum lifetime. The search for more accurate approximations for localized modes will be conducted in our future work.

There are two main parameters of the localizing function, the first is the degree of spatial localization, which should be found for a given DNVM amplitude, and the second is the position of the center of the localizing function with respect to the lattice. The importance of the second parameter was demonstrated by Page [3], who has found the DB centered between sites of a chain in addition to the DB centered on a lattice site reported by Sievers and Takeno [2].

For each DB described in Secs. V and VI, we give a single example, typically for a DNVM amplitude of 0.1 or 0.2. For the selected DNVM amplitude and the location of the DB center, the degree of spatial localization is determined by trial and error in order to obtain a DB with the maximum lifetime. To find the localization parameters of DBs for another DNVM amplitude, one should bear in mind the general trend according to which DBs of a smaller amplitude are less localized and, in the limit of vanishing amplitude, are transformed into delocalized phonons of a small amplitude, that is, into DNVMs of a small amplitude. Another important trend is that the instability of unstable DBs develops faster for a larger DNVM amplitude. This means that the unstable DBs with a smaller amplitude have a longer lifetime.

In the following paragraphs, zero-dimensional DBs localized in both spatial dimensions are described, followed by one-dimensional DBs localized in only one dimension. The initial conditions used to excite standing DBs imply that all particles have zero initial velocity, thus the total momentum transferred to the lattice is zero.

In the study of the zero-dimensional DBs, the computational cell size is  $N_x \times N_y = 256 \times 256$ , and absorbing boundary conditions are used in order to remove the radiation emitted at the early stage of the DB evolution. The one-dimensional DBs localized in the vertical (horizontal) direction are studied in the cell with  $N_x \times N_y = 8 \times 512$  ( $N_x \times N_y = 512 \times 8$ ) particles. Absorbing boundary conditions are imposed at the ends of the elongated cell.

### A. Zero-dimensional DB based on DNVM 2

For elastically anisotropic DNVM 2, the localizing function is taken in one of the possible forms as

$$A_{ij} = \frac{A}{\cosh[\beta_x(x_{ij} - x_0)] \cosh[\beta_y(y_{ij} - y_0)]}, \quad (32)$$

where  $A_{ij}$  is the magnitude of the initial displacement of the particle having coordinates  $(x_{ij}, y_{ij})$ ,  $A$  is the amplitude of DNVM 2, parameters  $\beta_x$  and  $\beta_y$  define the degree of the spatial localization of the DB in  $x$ - and  $y$ -direction, respectively, and  $(x_0, y_0)$  are the coordinates of the DB center.

An example of the DB based on the DNVM 2 is shown in Fig. 5. The parameters of the localizing function (32) are  $A = 0.1$ ,  $\beta_x = 0.8$ , and  $\beta_y = 0.7$ . The center of the localiz-

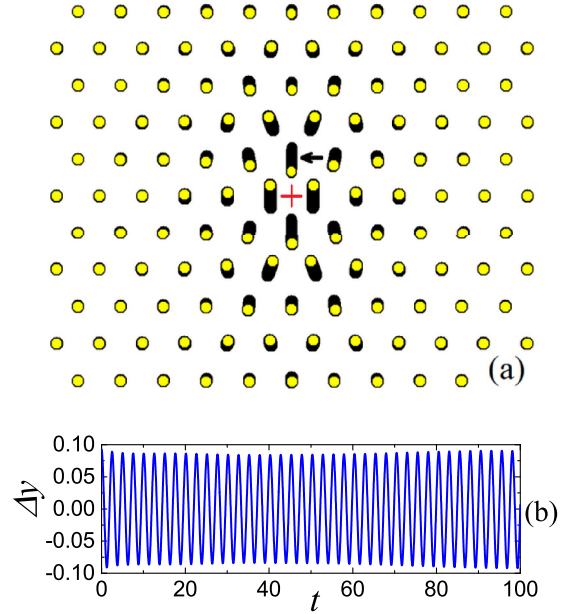


FIG. 5. (a) DB (shown by the red cross) based on the DNVM 2 centered between two particles in a horizontal close-packed row. Particle trajectories are shown in black. (b) Vertical displacement as a function of time for the particle indicated in (a) by the arrow. The DB was excited by the use of the localizing function (32) with  $A = 0.1$ ,  $\beta_x = 0.8$ , and  $\beta_y = 0.7$ . Displacements of the particles are scaled by a factor of 3.

ing function is placed between two particles in a horizontal close-packed row (see the red cross). We were unable to obtain a long-lived DB with a different center location. Figure 5(a) shows trajectories of the particles. The displacements of the particles are scaled by a factor of 3. The vertical displacement indicated by the arrow is plotted as a function of time in Fig. 5(b). The DB has a frequency  $\omega = 1.019\omega_{\max}$ , where  $\omega_{\max} = \sqrt{6}$  is the maximal phonon frequency.

The initial conditions used to excite the DB are imprecise, and some of the energy initially transferred to the localized mode is emitted. The pattern of DB vibrations is thus established. The presented DB has a relatively short lifetime of about 150 time units, after which it is destroyed due to instability. DBs excited with a smaller amplitude  $A$  have a longer lifetime and a frequency closer to  $\omega_{\max}$ .

### B. Zero-dimensional DBs based on DNVM 4

The DNVM 4 has a sixfold axis of symmetry, as the triangular lattice is elastically isotropic [113], meaning that long-wavelength phonons have direction-independent group velocity. Bearing this in mind, for the DNVM 4 the localizing function with radial symmetry is used:

$$A_{ij} = \frac{A}{\cosh(\beta|\mathbf{r}_{ij} - \mathbf{r}_0|)}, \quad (33)$$

where  $A_{ij}$  is the magnitude of the initial displacement of the particle having radius-vector  $\mathbf{r}_{ij} = (x_{ij}, y_{ij})$ ,  $A$  is the amplitude of the DNVM 4, parameter  $\beta$  defines the degree of the spatial localization of the DB, and  $\mathbf{r}_0$  is the radius-vector of the center of the localizing function.

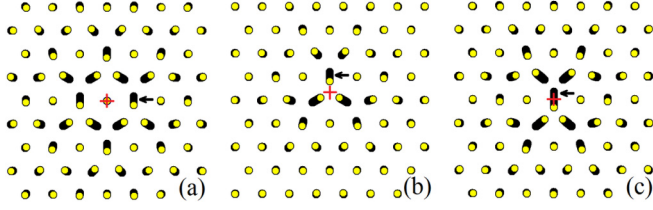


FIG. 6. DBs obtained by applying the localizing function (33) upon DNVM 4 with the amplitude  $A = 0.1$ . Depending on the location of the center of the localizing function  $\mathbf{r}_0$  shown by the red crosses, (a) six-, (b) three-, or (c) twofold symmetry DBs are obtained. Stable long-lived oscillations are observed for (a)  $\beta = 0.830$ , (b)  $\beta = 0.730$ , and (c)  $\beta = 0.838$  (Fig. 7). Particle trajectories are shown in black. Displacements of the particles are scaled by a factor of 3.

Examples of DBs are given in Fig. 6 with different locations of the center of the localizing function (marked with the red crosses). The center is located on a resting particle in Fig. 6(a), in the middle of triangle made by the moving particles in Fig. 6(b), and on the lattice site of a moving particle in Fig. 6(c). The DBs have sixfold, threefold, and twofold symmetry axes, respectively, in the three subfigures. Parameters of the localizing function (33) are  $\beta = 0.830$ ,  $\beta = 0.730$ , and  $\beta = 0.838$ , respectively. The DNVM amplitude is  $A = 0.1$  in all the cases. For clarity, the displacements of the particles are scaled by a factor of 3. With the chosen parameters, the DBs practically do not radiate energy and have very long lifetime. The displacement of the particle vibrating with the largest amplitude as the function of time is shown in Figs. 7(a)–7(c) for the DBs presented in Figs. 6(a)–6(c), respectively. The DBs have frequencies  $\omega = 1.008\omega_{\max}$ ,  $\omega = 1.018\omega_{\max}$ , and  $\omega = 1.017\omega_{\max}$ , respectively, where  $\omega_{\max} = \sqrt{6}$ .

The DB with the sixfold symmetry axis shown in Fig. 6(a) has been observed earlier in triangular Morse lattices with an on-site harmonic potential [89] and without on-site potential [104].

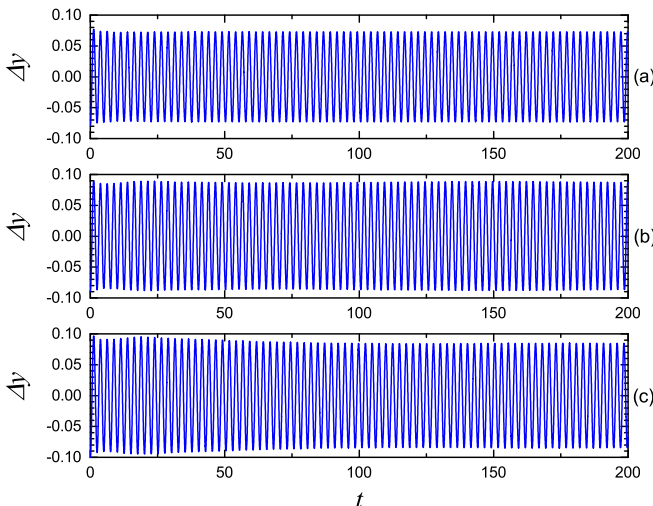


FIG. 7. (a–c) Displacements along the y-axis of particles marked by the arrows in Figs. 6(a)–6(c), respectively.

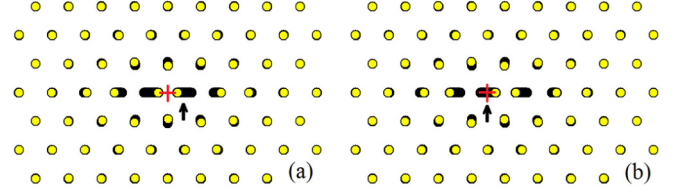


FIG. 8. DBs based on the DNVM  $\gamma 2$ . DBs were obtained by applying the localizing function (32) upon DNVM  $\gamma 2$  with the amplitude  $A = 0.2$ . The center of the localizing function is shown by the red crosses. In (a) it is between particles vibrating horizontally and in (b) on a particle vibrating horizontally. Stable long-lived oscillations in both cases are observed for  $\beta_x = 1.35$  and  $\beta_y = 1.10$ . Particle trajectories are shown in black. Particle displacements are multiplied by a factor of 1.5.

### C. Zero-dimensional DBs based on DNVM $\gamma 2$

Since the DNVM  $\gamma 2$  is anisotropic, the localizing function (32) is used. Two examples of DBs obtained from the time-periodic DNVM  $\gamma 2$  are presented in Fig. 8. They were obtained by placing the center of the localizing function between horizontally vibrating particles and on a horizontally vibrating particle, respectively. In both cases,  $A = 0.2$ ,  $\beta_x = 1.35$ , and  $\beta_y = 1.10$ .

Displacements of particles marked by the arrows in Figs. 8(a) and 8(b) along the  $x$ -axis are shown as functions of time in Figs. 9(a) and 9(b), respectively. The DBs have very long lifetime and show no signs of instability. They have frequencies  $\omega = 1.069\omega_{\max}$  and  $\omega = 1.072\omega_{\max}$ , respectively.

The previous works [89,114] showed that the DBs based on the DNVM  $\gamma 2$  were robust and could propagate along close-packed rows of particles and survive collisions with each other [114]. Here we do not analyze motion of this particular DB.

### D. One-dimensional DBs based on DNVMs of the triangular lattice

One-dimensional horizontal DBs (localized in vertical direction and delocalized in horizontal direction) are excited by imposing the following localizing function on a DNVM:

$$A_{ij} = \frac{A}{\cosh[\beta_y(y_{ij} - y_0)]}, \quad (34)$$

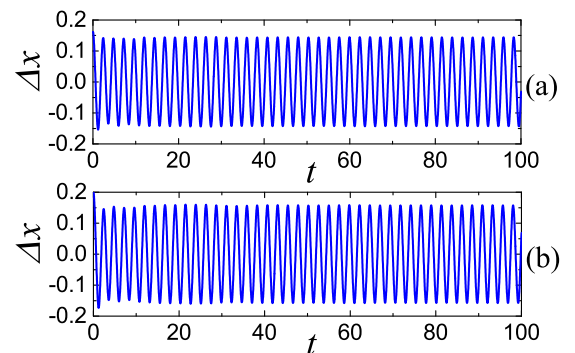


FIG. 9. (a, b) Displacements along the  $x$ -axis of particles marked by the arrows in Figs. 8(a) and 8(b), respectively.

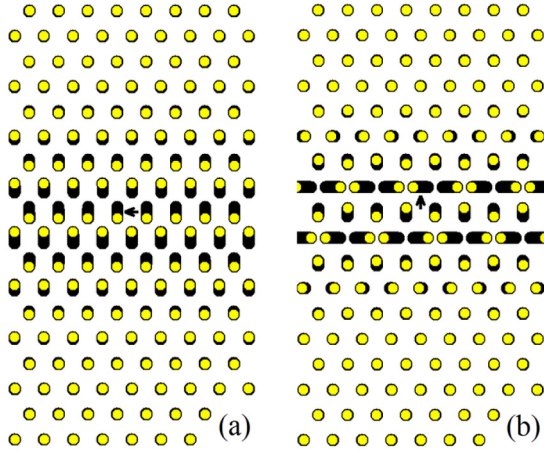


FIG. 10. One-dimensional horizontal DBs based on (a) DNVM 2 and (b) DNVM  $\gamma 2$ , obtained by applying the localizing function (34) upon DNVMs with the amplitude  $A = 0.1$ . Long-lived oscillations are observed for (a)  $\beta_x = 0.65$  and (b)  $\beta_x = 0.79$ . Particle trajectories are shown in black. Displacements of the particles are magnified by a factor of 3.

where  $A_{ij}$  is the magnitude of the initial displacement of the particle having a  $y$ -coordinate  $y_{ij}$ ,  $A$  is the amplitude of the DNVM, parameter  $\beta_y$  defines the degree of the spatial localization of the DB, and  $y_0$  is the  $y$ -coordinate of the maximum of the localizing function.

Similarly, one-dimensional vertical DBs (localized only in horizontal direction) are excited by imposing a localizing function of the form

$$A_{ij} = \frac{A}{\cosh[\beta_x(x_{ij} - x_0)]}, \quad (35)$$

on a DNVM, where  $A_{ij}$  is the magnitude of the initial displacement of the particle having  $x$ -coordinate  $x_{ij}$ ,  $A$  is the amplitude of DNVM, parameter  $\beta_x$  defines the degree of the spatial localization of the DB, and  $x_0$  is the  $x$ -coordinate of the maximum of the localizing function.

Examples of one-dimensional horizontal DBs are shown in Fig. 10. They are obtained by imposing localizing function (34) on (a) DNVM 2 and (b) DNVM  $\gamma 2$ . In both cases, the delocalized modes have amplitude  $A = 0.1$ . The localizing function is placed such that its maximum is between two horizontal close-packed rows for Fig. 10(a) and in a horizontal row with vertically vibrating particles for Fig. 10(b).  $\beta_x = 0.65$  and  $\beta_x = 0.79$  respectively in the two cases. These two DBs lose their energy due to the very slow radiation, and thus have a very long lifetime. On the other hand, DNVM 4 creates an unstable DB with a lifetime of a few tens of oscillation periods. We do not present this short-lived DB here.

Displacements of particles indicated by the arrows in Figs. 10(a) and 10(b) are shown as functions of time in Figs. 11(a) and 11(b), respectively. The DB frequencies are  $\omega = 1.046\omega_{\max}$  and  $\omega = 1.049\omega_{\max}$ , respectively.

Figures 12(a)–12(c) shows examples of one-dimensional vertical DBs based on DNVM 2, DNVM 4, and DNVM  $\gamma 2$ , respectively. In all cases, the DNVM amplitude is  $A = 0.1$ . DBs with long lifetime are observed for (a)  $\beta_x = 1.15$ , (b)  $\beta_x = 1.07$ , and (c)  $\beta_x = 0.687$ . Displacements of particles in-

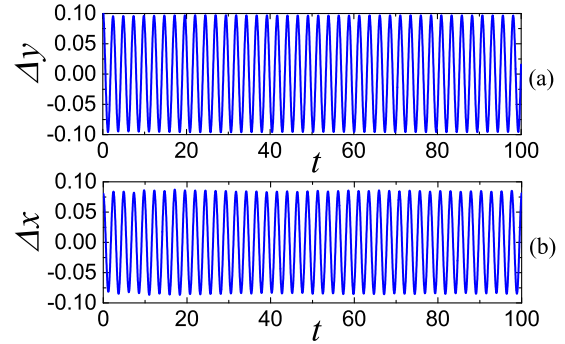


FIG. 11. (a, b) Displacements of particles indicated by the arrows in Figs. 10(a) and 10(b), respectively. (a) Along the  $y$ -axis and (b) along the  $x$ -axis as functions of time

indicated by the arrows are shown as functions of time (Fig. 13). Figures 13(a) and 13(b) present displacements along the  $y$ -axis, and Fig. 13(c) shows the displacement along the  $x$ -axis. The DBs have frequencies  $\omega = 1.048\omega_{\max}$ ,  $\omega = 1.041\omega_{\max}$ , and  $\omega = 1.039\omega_{\max}$ , respectively.

The DBs presented in Fig. 12(a) and 12(c) show no sign of instability, while the one shown in Fig. 12(b) has relatively short lifetime.

As far as we know, one-dimensional DBs based on the DNVMs of a triangular lattice as presented above have not been described in the literature and are hence innovative discoveries.

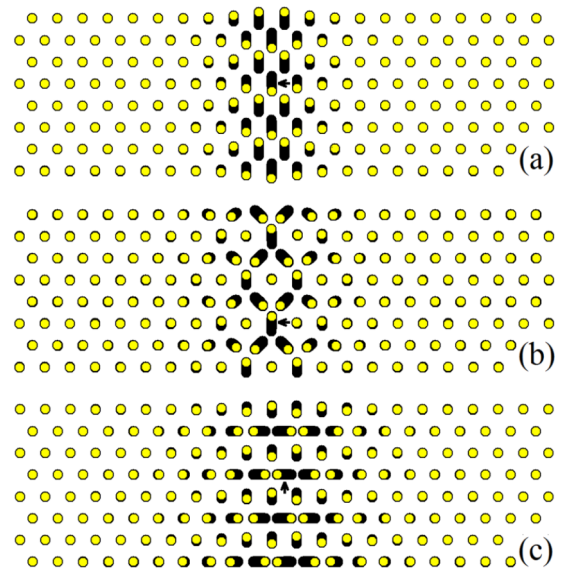


FIG. 12. One-dimensional vertical DBs based on (a) DNVM 2, (b) DNVM 4, and (c) DNVM  $\gamma 2$ , obtained by applying the localizing function (35) upon DNVMs with the amplitude  $A = 0.1$ . Long-lived oscillations are observed for (a)  $\beta_x = 1.15$ , (b)  $\beta_x = 1.07$ , and (c)  $\beta_x = 0.687$ . Particle trajectories are shown in black. Displacements of the particles are magnified by a factor of 3.

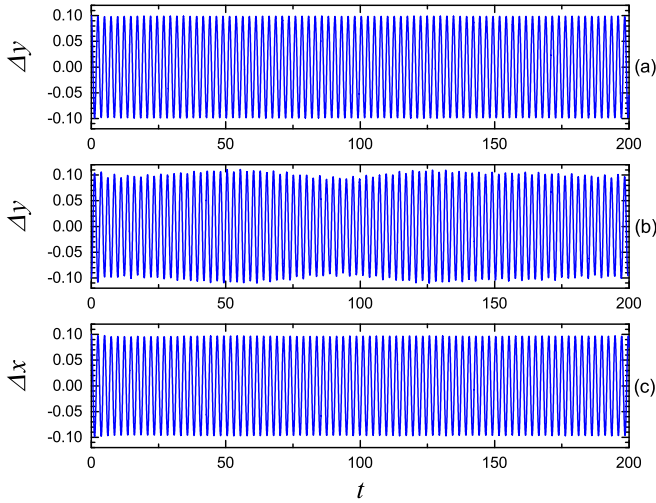


FIG. 13. (a)-(c) Displacements as functions of time for particles indicated by the arrows in Figs. 12(a)–12(c), respectively. The displacements in (a) and (b) are along the  $y$ -axis and the displacements in (c) are along the  $x$ -axis.

**VI. DISCRETE BREATHERS BASED ON DNVMs OF A CHAIN**

In Sec. I, it was mentioned that nonlinear chains support one-component DNVMs with periodic patterns  $[A, -A]$ ,  $[A, 0, -A]$ ,  $[A, 0, -A, 0]$ , and  $[A, A, -A, -A]$ , where  $A$  is the DNVM amplitude [95]. In this section, it is demonstrated that the modes  $[A, -A]$  and  $[A, 0, -A, 0]$  can be excited in a close-packed row of the  $\beta$ -FPUT lattice.

Figure 14 presents the initial displacement patterns (a)  $[A, -A]$  and (b)  $[A, 0, -A, 0]$ . Only particles in one atomic row are initially displaced according to these patterns, and

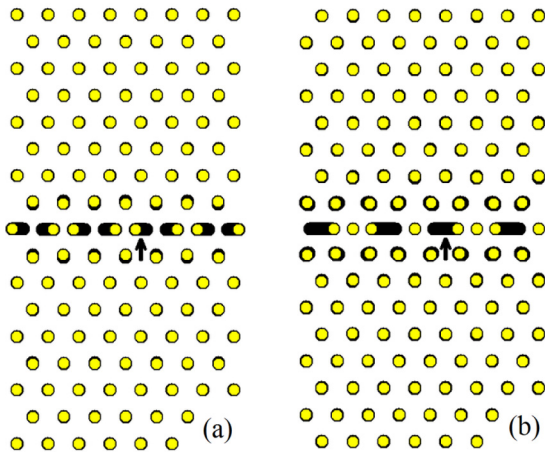


FIG. 14. One-dimensional DBs based on DNVMs of a chain, which have periodic patterns (a)  $[A, -A]$  and (b)  $[A, 0, -A, 0]$ . The DBs are excited by introducing initial displacements to the particles in a close-packed row according to these patterns. Spatially localized oscillations are observed with (a)  $A = 0.2$  and (b)  $A = 0.8$ . Particle trajectories are shown in black. The particle displacements in (b) are scaled by a factor of 0.5 to prevent trajectory overlapping of particles vibrating with large amplitudes.

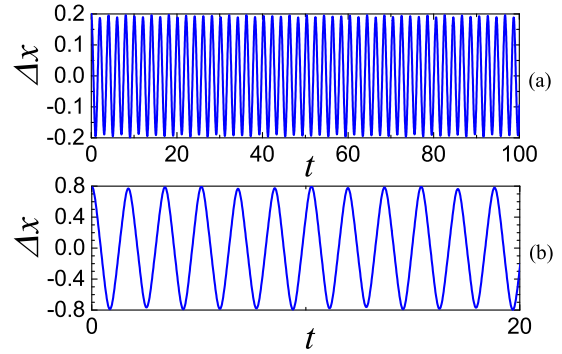


FIG. 15. (a), (b) Displacements  $\Delta x$  as functions of time for particles indicated by the arrows in Figs. 14(a) and 14(b), respectively.

initial velocities of all the particles are set equal to zero. Spatially localized oscillations are observed with  $A = 0.2$  for Fig. 14(a) and  $A = 0.8$  for Fig. 14(b). In the former case, the DB has a very long lifetime with practically no energy emission. In the latter case, the lifetime of the DB is limited to a few tens of oscillation periods. This observation is because the oscillations have frequencies above the phonon spectrum with only very large amplitudes, where the instability of the mode develops very rapidly.

It should be pointed out that the one-dimensional DB shown in Fig. 14(b) can be excited by imposing the localizing function (34) upon the DNVM  $\gamma_2$  with the center localized in a row with horizontally vibrating particles, as contrasted to the one located in a row with vertically vibrating particles in Fig. 10(b).

Importantly, this DB cannot have an amplitude smaller than a certain value because the DNVM  $[A, 0, -A, 0]$  would have frequencies within the phonon band at small amplitudes. All the other DBs presented in this work have frequencies bifurcating from the upper edge of the phonon spectrum.

Horizontal displacements of the particles indicated with the arrows are plotted as functions of time in Fig. 15. The DNVM frequencies are (a)  $\omega = 1.27\omega_{\max}$  and (b)  $\omega = 1.50\omega_{\max}$ , which are above the upper edge of the phonon band.

**VII. CONCLUSIONS AND FUTURE CHALLENGES**

A list of (quasi-) DBs of the triangular  $\beta$ -FPUT lattice was described with frequencies bifurcating from the upper edge of the phonon band. The zero- and one-dimensional DBs were obtained by localizing DNVMs of the triangular lattice with frequencies above the phonon band.

One example of a DB with the frequency emerging from the phonon band at a relatively large amplitude was given; see Fig. 14(b). This breather is obtained by exciting the DNVM of a chain in a close-packed row of particles. The breather exists only at a relatively large amplitude and has a very short lifetime due to the rapidly developing instability. Other short-lived breathers can possibly exist based on DNVMs of the triangular lattice with frequencies emerging from the phonon spectrum at large amplitudes [94]. Examples of such DBs were reported for bcc metals in [106].

We did not try to find exact DB solutions in this work, but they can probably be found using iterative or other methods,

for example, the generalized minimal residual method [111] or asymptotic analysis used in [115].

Some DBs in two-dimensional lattices can move [62,63,114] and in one of our future works we will address the problem of mobility for the DBs presented in this work.

For a triangular lattice with different potentials, for example, an  $\alpha$ - $\beta$ -FPUT lattice or a Morse lattice, one should start by analyzing the frequency-amplitude dependences of DNVMs listed in [94]. All DNVMs described in this paper exist in triangular lattices with any type of potential, but properties such as DNVM frequencies depend on the potential. DNVMs with frequencies higher than the phonon band are candidates for obtaining DBs by imposing localizing functions by analogy with this work.

In a triangular lattice with an on-site potential, gap DBs are possible [115], which were not considered in our work. But they can be described using the same approach, and this is planned to be done in a forthcoming study.

Using the approach presented in this work, one can search for a complete list of DBs in metals with fcc, bcc, and hcp structures and in other crystals with a more complex structure. All DNVMs with frequencies above the phonon spectrum should be derived to reveal the complete list of DBs.

## ACKNOWLEDGMENTS

The authors acknowledge the financial support from Nanyang Environment & Water Research Institute. Research of E.G.S. was carried out at National Research Tomsk Polytechnic University within the framework of a Tomsk Polytechnic University Competitiveness Enhancement Program grant.

- 
- [1] A. S. Dolgov, On localization of oscillations in nonlinear crystal structure, *Sov. Phys. Solid State* **28**, 907 (1986).
- [2] A. J. Sievers and S. Takeno, Intrinsic Localized Modes in Anharmonic Crystals, *Phys. Rev. Lett.* **61**, 970 (1988).
- [3] J. B. Page, Asymptotic solutions for localized vibrational modes in strongly anharmonic periodic systems, *Phys. Rev. B* **41**, 7835 (1990).
- [4] S. Flach and C. R. Willis, Discrete breathers, *Phys. Rep.* **295**, 181 (1998).
- [5] S. Flach and A. V. Gorbach, Discrete breathers—Advances in theory and applications, *Phys. Rep.* **467**, 1 (2008).
- [6] S. V. Dmitriev, E. A. Korznikova, J. A. Baimova, and M. G. Velarde, Discrete breathers in crystals, *Phys. Usp.* **59**, 446 (2016).
- [7] M. Sato, B. E. Hubbard, and A. J. Sievers, Nonlinear energy localization and its manipulation in micromechanical oscillator arrays, *Rev. Mod. Phys.* **78**, 137 (2006).
- [8] M. Sato, B. E. Hubbard, A. J. Sievers, B. Ilic, and H. G. Craighead, Optical manipulation of intrinsic localized vibrational energy in cantilever arrays, *Europhys. Lett.* **66**, 318 (2004).
- [9] M. Sato, B. E. Hubbard, A. J. Sievers, B. Ilic, D. A. Czaplewski, and H. G. Craighead, Observation of Locked Intrinsic Localized Vibrational Modes in a Micromechanical Oscillator Array, *Phys. Rev. Lett.* **90**, 044102 (2003).
- [10] E. Trias, J. J. Mazo, and T. P. Orlando, Discrete Breathers in Nonlinear Lattices: Experimental Detection in a Josephson Array, *Phys. Rev. Lett.* **84**, 741 (2000).
- [11] P. Binder, D. Abramov, A. V. Ustinov, S. Flach, and Y. Zolotaryuk, Observation of Breathers in Josephson Ladders, *Phys. Rev. Lett.* **84**, 745 (2000).
- [12] F. Palmero, L. Q. English, X.-L. Chen, W. Li, J. Cuevas-Maraver, and P. G. Kevrekidis, Experimental and numerical observation of dark and bright breathers in the band gap of a diatomic electrical lattice, *Phys. Rev. E* **99**, 032206 (2019).
- [13] A. Gomez-Rojas and P. Halevi, Discrete breathers in an electric lattice with an impurity: Birth, interaction, and death, *Phys. Rev. E* **97**, 022225 (2018).
- [14] Y. Watanabe, T. Nishida, Y. Doi, and N. Sugimoto, Experimental demonstration of excitation and propagation of intrinsic localized modes in a mass-spring chain, *Phys. Lett. A* **382**, 1957 (2018).
- [15] J. Cuevas, L. Q. English, P. G. Kevrekidis, and M. Anderson, Discrete Breathers in a Forced-Damped Array of Coupled Pendula: Modeling, Computation, and Experiment, *Phys. Rev. Lett.* **102**, 224101 (2009).
- [16] F. M. Russell, Y. Zolotaryuk, J. C. Eilbeck, and T. Dauxois, Moving breathers in a chain of magnetic pendulums, *Phys. Rev. B* **55**, 6304 (1997).
- [17] K. Vorotnikov, Y. Starosvetsky, G. Theocharis, and P. G. Kevrekidis, Wave propagation in a strongly nonlinear locally resonant granular crystal, *Physica D* **365**, 27 (2018).
- [18] C. Chong, M. A. Porter, P. G. Kevrekidis, and C. Daraio, Nonlinear coherent structures in granular crystals, *J. Phys.: Condens. Matter* **29**, 413003 (2017).
- [19] M. E. Manley, A. J. Sievers, J. W. Lynn, S. A. Kiselev, N. I. Agladze, Y. Chen, A. Llobet, and A. Alatas, Intrinsic localized modes observed in the high-temperature vibrational spectrum of NaI, *Phys. Rev. B* **79**, 134304 (2009).
- [20] M. E. Manley, D. L. Abernathy, N. I. Agladze, and A. J. Sievers, Symmetry-breaking dynamical pattern and localization observed in the equilibrium vibrational spectrum of NaI, *Sci. Rep.* **1**, 4 (2011).
- [21] S. A. Kiselev and A. J. Sievers, Generation of intrinsic vibrational gap modes in three-dimensional ionic crystals, *Phys. Rev. B* **55**, 5755 (1997).
- [22] L. Z. Khadeeva and S. V. Dmitriev, Discrete breathers in crystals with NaCl structure, *Phys. Rev. B* **81**, 214306 (2010).
- [23] A. Riviere, S. Lepri, D. Colognesi, and F. Piazza, Wavelet imaging of transient energy localization in nonlinear systems at thermal equilibrium: The case study of NaI crystals at high temperature, *Phys. Rev. B* **99**, 024307 (2019).
- [24] N. K. Voulgarakis, G. Hadjisavvas, P. C. Kelires, and G. P. Tsironis, Computational investigation of intrinsic localization in crystalline Si, *Phys. Rev. B* **69**, 113201 (2004).
- [25] R. T. Murzaev, D. V. Bachurin, E. A. Korznikova, and S. V. Dmitriev, Localized vibrational modes in diamond, *Phys. Lett. A* **381**, 1003 (2017).

- [26] M. Haas, V. Hizhnyakov, A. Shelkan, M. Klopov, and A. J. Sievers, Prediction of high-frequency intrinsic localized modes in Ni and Nb, *Phys. Rev. B* **84**, 144303 (2011).
- [27] O. V. Bachurina and A. A. Kudreyko, Two-dimensional discrete breathers in fcc metals, *Comp. Mater. Sci.* **182**, 109737 (2020).
- [28] O. V. Bachurina, Plane and plane-radial discrete breathers in fcc metals, *Model. Simul. Mater. Sci.* **27**, 055001 (2019).
- [29] O. V. Bachurina, Linear discrete breather in fcc metals, *Comp. Mater. Sci.* **160**, 217 (2019).
- [30] O. V. Bachurina, R. T. Murzaev, A. S. Semenov, E. A. Korznikova, and S. V. Dmitriev, Properties of moving discrete breathers in beryllium, *Phys. Solid State* **60**, 989 (2018).
- [31] R. T. Murzaev, A. A. Kistanov, V. I. Dubinko, D. A. Terentyev, and S. V. Dmitriev, Moving discrete breathers in bcc metals V, Fe and W, *Comp. Mater. Sci.* **98**, 88 (2015).
- [32] D. A. Terentyev, A. V. Dubinko, V. I. Dubinko, S. V. Dmitriev, E. E. Zhurkin, and M. V. Sorokin, Interaction of discrete breathers with primary lattice defects in bcc Fe, *Model. Simul. Mater. Sci.* **23**, 085007 (2015).
- [33] M. E. Manley, M. Yethiraj, H. Sinn, H. M. Volz, A. Alatas, J. C. Lashley, W. L. Hults, G. H. Lander, and J. L. Smith, Formation of a New Dynamical Mode in  $\alpha$ -Uranium Observed by Inelastic X-Ray and Neutron Scattering, *Phys. Rev. Lett.* **96**, 125501 (2006).
- [34] R. T. Murzaev, R. I. Babicheva, K. Zhou, E. A. Korznikova, S. Y. Fomin, V. I. Dubinko, and S. V. Dmitriev, Discrete breathers in alpha-uranium, *Eur. Phys. J. B* **89**, 168 (2016).
- [35] V. Dubinko, D. Laptev, D. Terentyev, S. V. Dmitriev, and K. Irwin, Assessment of discrete breathers in the metallic hydrides, *Comp. Mater. Sci.* **158**, 389 (2019).
- [36] P. V. Zakharov, E. A. Korznikova, S. V. Dmitriev, E. G. Ekomasov, and K. Zhou, Surface discrete breathers in Pt<sub>3</sub>Al intermetallic alloy, *Surf. Sci.* **679**, 1 (2019).
- [37] M. D. Starostenkov, A. I. Potekaev, S. V. Dmitriev, P. V. Zakharov, A. M. Eremin, and V. V. Kulagina, Dynamics of discrete breathers in a Pt<sub>3</sub>Al crystal, *Russ. Phys. J.* **58**, 1353 (2016).
- [38] N. N. Medvedev, M. D. Starostenkov, and M. E. Manley, Energy localization on the Al sublattice of Pt<sub>3</sub>Al with L12 order, *J. Appl. Phys.* **114**, 213506 (2013).
- [39] J. A. Baimova, E. A. Korznikova, I. P. Lobzenko, and S. V. Dmitriev, Discrete breathers in carbon and hydrocarbon nanostructures, *Rev. Adv. Mater. Sci.* **42**, 68 (2015).
- [40] B. Liu, J. A. Baimova, S. V. Dmitriev, X. Wang, H. Zhu, K. Zhou, Discrete breathers in hydrogenated graphene, *J. Phys. D: Appl. Phys.* **46**, 305302 (2013).
- [41] E. A. Korznikova, J. A. Baimova, and S. V. Dmitriev, Effect of strain on gap discrete breathers at the edge of armchair graphene nanoribbons, *Europhys. Lett.* **102**, 60004 (2013).
- [42] J. A. Baimova, S. V. Dmitriev, and K. Zhou, Discrete breather clusters in strained graphene, *Europhys. Lett.* **100**, 36005 (2012).
- [43] E. A. Korznikova, A. V. Savin, Y. A. Baimova, S. V. Dmitriev, and R. R. Mulyukov, Discrete breather on the edge of the graphene sheet with the armchair orientation, *JETP Lett.* **96**, 222 (2012).
- [44] A. V. Savin and Y. S. Kivshar, Nonlinear breatherlike localized modes in C60 nanocrystals, *Phys. Rev. B* **85**, 125427 (2012).
- [45] Y. Yamayose, Y. Kinoshita, Y. Doi, A. Nakatani, and T. Kitamura, Excitation of intrinsic localized modes in a graphene sheet, *Europhys. Lett.* **80**, 40008 (2007).
- [46] T. Shimada, D. Shirasaki, and T. Kitamura, Stone-Wales transformations triggered by intrinsic localized modes in carbon nanotubes, *Phys. Rev. B* **81**, 035401 (2010).
- [47] Y. Kinoshita, Y. Yamayose, Y. Doi, A. Nakatani, and T. Kitamura, Selective excitations of intrinsic localized modes of atomic scales in carbon nanotubes, *Phys. Rev. B* **77**, 024307 (2008).
- [48] Y. Doi and A. Nakatani, Numerical study on unstable perturbation of intrinsic localized modes in graphene, *J. Solid Mechanics Mater. Eng.* **6**, 71 (2012).
- [49] L. Z. Khadeeva, S. V. Dmitriev, and Y. S. Kivshar, Discrete breathers in deformed graphene, *JETP Lett.* **94**, 539 (2011).
- [50] E. Barani, I. P. Lobzenko, E. A. Korznikova, E. G. Soboleva, S. V. Dmitriev, K. Zhou, and A. M. Marjaneh, Transverse discrete breathers in unstrained graphene, *Eur. Phys. J. B* **90**, 38 (2017).
- [51] I. Evazzade, I. P. Lobzenko, E. A. Korznikova, I. A. Ovid'Ko, M. R. Roknabadi, and S. V. Dmitriev, Energy transfer in strained graphene assisted by discrete breathers excited by external ac driving, *Phys. Rev. B* **95**, 035423 (2017).
- [52] E. Barani, E. A. Korznikova, A. P. Chetverikov, K. Zhou, and S. V. Dmitriev, Gap discrete breathers in strained boron nitride, *Phys. Lett. A* **381**, 3553 (2017).
- [53] A. P. Chetverikov, K. S. Sergeev, and V. D. Lakhno, Trapping and transport of charges in DNA by mobile discrete breathers, *Math. Biol. Bioinf.* **13**, t59 (2018).
- [54] F. Piazza and Y.-H. Sanejouand, Discrete breathers in protein structures, *Phys. Biol.* **5**, 026001 (2008).
- [55] B. Juanico, Y.-H. Sanejouand, F. Piazza, and P. De Los Rios, Discrete Breathers in Nonlinear Network Models of Proteins, *Phys. Rev. Lett.* **99**, 238104 (2007).
- [56] M. Peyrard, S. Cuesta-Lopez, and G. James, Nonlinear analysis of the dynamics of DNA breathing, *J. Biol. Phys.* **35**, 73 (2009).
- [57] C. L. Gninzanlong, F. T. Ndjomatchoua, and C. Tchawoua, Forward and backward propagating breathers in a DNA model with dipole-dipole long-range interactions, *Phys. Rev. E* **102**, 052212 (2020).
- [58] G. M. Chechin, G. S. Dzhelauhova, and E. A. Mehonoshina, Quasibreathers as a Generalization of the Concept of Discrete Breathes, *Phys. Rev. E* **74**, 036608 (2006).
- [59] A. Shelkan, M. Klopov, and V. Hizhnyakov, Enhanced mobility of high-frequency discrete breathers in a monatomic chain with odd anharmonicity, *Phys. Lett. A* **383**, 1893 (2019).
- [60] Y. Doi and K. Yoshimura, Construction of nonlinear lattice with potential symmetry for smooth propagation of discrete breather, *Nonlinearity* **33**, 5142 (2020).
- [61] Y. Doi and K. Yoshimura, Symmetric Potential Lattice and Smooth Propagation of Tail-Free Discrete Breathes, *Phys. Rev. Lett.* **117**, 014101 (2016).
- [62] J. L. Marín, F. M. Russell, and J. C. Eilbeck, Breathes in cuprate-like lattices, *Phys. Lett. A* **281**, 21 (2001).
- [63] J. L. Marín, J. C. Eilbeck, and F. M. Russell, Localized moving breathes in a 2D hexagonal lattice, *Phys. Lett. A* **248**, 225 (1998).
- [64] F. Hadipour, D. Saadatmand, M. Ashhadi, A. Moradi Marjaneh, I. Evazzade, A. Askari, and S. V. Dmitriev, Interaction of phonons with discrete breathes in one-dimensional

- chain with tunable type of anharmonicity, *Phys. Lett. A* **384**, 126100 (2020).
- [65] D. Saadatmand, D. Xiong, V. A. Kuzkin, A. M. Krivtsov, A. V. Savin, and S. V. Dmitriev, Discrete breathers assist energy transfer to ac-driven nonlinear chains, *Phys. Rev. E* **97**, 022217 (2018).
- [66] D. Xiong, D. Saadatmand, and S. V. Dmitriev, Crossover from ballistic to normal heat transport in the  $\phi^4$  lattice: If nonconservation of momentum is the reason, what is the mechanism? *Phys. Rev. E* **464**, 042109 (2017).
- [67] J. Wang, S. V. Dmitriev, and D. Xiong, Thermal transport in long-range interacting Fermi-Pasta-Ulam chains, *Phys. Rev. Research* **2**, 013179 (2020).
- [68] M. E. Manley, Impact of intrinsic localized modes of atomic motion on materials properties, *Acta Mater.* **58**, 2926 (2010).
- [69] E. A. Korznikova, A. Y. Morkina, M. Singh, A. M. Krivtsov, V. A. Kuzkin, V. A. Gani, Yu. V. Bebikhov, and S. V. Dmitriev, Effect of discrete breathers on macroscopic properties of the Fermi-Pasta-Ulam chain, *Eur. Phys. J. B* **93**, 123 (2020).
- [70] M. E. Manley, M. Yethiraj, H. Sinn, H. M. Volz, A. Alatas, J. C. Lashley, W. L. Hulst, G. H. Lander, D. J. Thoma, and J. L. Smith, Intrinsically localized vibrations and the mechanical properties of  $\alpha$ -uranium, *J. Alloy. Compd.* **444**, 129 (2007).
- [71] B. Mihaila, C. P. Opeil, F. R. Drymiotis, J. L. Smith, J. C. Cooley, M. E. Manley, A. Migliori, C. Mielke, T. Lookman, A. Saxena *et al.*, Pinning Frequencies of the Collective Modes in  $\alpha$ -Uranium, *Phys. Rev. Lett.* **96**, 076401 (2006).
- [72] M. Singh, A. Y. Morkina, E. A. Korznikova, V. I. Dubinko, D. A. Terentiev, D. Xiong, O. B. Naimark, V. A. Gani, and S. V. Dmitriev, Effect of discrete breathers on the specific heat of a nonlinear chain, *J. Nonlinear Sci.* **31**, 12 (2021).
- [73] A. P. Chetverikov, W. Ebeling, V. D. Lakhno, and M. G. Velarde, Discrete-breather-assisted charge transport along DNA-like molecular wires, *Phys. Rev. E* **100**, 052203 (2019).
- [74] Z. Zhu, P. A. Maksimov, S. R. White, and A. L. Chernyshev, Topography of spin liquids on a triangular lattice, *Phys. Rev. Lett.* **120**, 207203 (2018).
- [75] K. A. Krylova, E. A. Korznikova, A. S. Semenov, D. V. Bachurin, and S. V. Dmitriev, Linking tracks in mica crystals with phase transitions in a bistable lattice, *Eur. Phys. J. B* **93**, 23 (2020).
- [76] F. M. Russell and J. C. Eilbeck, Evidence for moving breathers in a layered crystal insulator at 300 K, *Europhys. Lett.* **78**, 10004 (2007).
- [77] J. Bajars, J. C. Eilbeck, B. Leimkuhler, Nonlinear propagating localized modes in a 2D hexagonal crystal lattice, *Physica D* **301**, 8 (2015).
- [78] J. Bajars, J. C. Eilbeck, and B. Leimkuhler, Numerical simulations of nonlinear modes in mica: Past, present and future, in *Quodons in Mica*, edited by J. Archilla, N. Jimenez, V. Sanchez-Morcillo, and L. Garcia-Raffi, Springer Series in Materials Science Vol. 21 (Springer, Cham, 2015), p. 35.
- [79] F. Wang and A. Vishwanath, Spin-liquid states on the triangular and Kagomé lattices: A projective-symmetry-group analysis of Schwinger boson states, *Phys. Rev. B* **74**, 174423 (2006).
- [80] Y. Sun, Z. Zhuo, X. Wu, and J. Yang, Room-temperature ferromagnetism in two-dimensional  $\text{Fe}_2\text{Si}$  nanosheet with enhanced spin-polarization ratio, *Nano Lett.* **17**, 2771 (2017).
- [81] Y. Peng, W. Li, F. Wang, T. Still, A. G. Yodh, and Y. Han, Diffusive and martensitic nucleation kinetics in solid-solid transitions of colloidal crystals, *Nat. Commun.* **8**, 14978 (2017).
- [82] V. A. Kuzkin, A. M. Krivtsov, E. A. Podolskaya, and M. L. Kachanov, Lattice with vacancies: Elastic fields and effective properties in frameworks of discrete and continuum models, *Philos. Mag.* **96**, 1538 (2016).
- [83] C. Chong, Y. Wang, D. Marechal, E. G. Charalampidis, M. Moleron, A. J. Martnez, M. A. Porter, P. G. Kevrekidis, and C. Daraio, Nonlinear localized modes in two-dimensional hexagonally-packed magnetic lattices, *New J. Phys.* **23**, 043008 (2021).
- [84] X. Yi and S. Liu, Stationary breather model in a two-dimensional hexagonal spring-mass lattice, *Nucl. Phys. B* **951**, 114884 (2020).
- [85] A. P. Chetverikov, W. Ebeling, and M. G. Velarde, Localized nonlinear, soliton-like waves in two-dimensional anharmonic lattices, *Wave Motion* **48**, 753 (2011).
- [86] A. P. Chetverikov, W. Ebeling, and M. G. Velarde, Nonlinear soliton-like excitations in two-dimensional lattices and charge transport, *Eur. Phys. J.: Special Topics* **222**, 2531 (2013).
- [87] I. G. Bostrem, E. G. Ekomasov, J.-I. Kishine, A. S. Ovchinnikov, and V. E. Sinityn, Discrete magnetic breathers in monoaxial chiral helimagnet, *Chelyab. Fiz.-Mat. Zh.* **5**, 194 (2020).
- [88] B.-B. Lü and Q. Tian, Discrete breathers in a two-dimensional Morse lattice with an on-site harmonic potential, *Front. Phys. China* **4**, 497 (2009).
- [89] K. Ikeda, Y. Doi, B.-F. Feng, and T. Kawahara, Chaotic breathers of two types in a two-dimensional Morse lattice with an on-site harmonic potential, *Physica D* **225**, 184 (2007).
- [90] V. Koukouloyannis and R. S. MacKay, Existence and stability of 3-site breathers in a triangular lattice, *J. Phys. A: Math. Gen.* **38**, 1021 (2005).
- [91] V. Koukouloyannis, P. G. Kevrekidis, K. J. H. Law, I. Kourakis, and D. J. Frantzeskakis, Existence and stability of multisite breathers in honeycomb and hexagonal lattices, *J. Phys. A: Math. Theor.* **43**, 235101 (2010).
- [92] I. A. Butt and J. A. D. Wattis, Discrete breathers in a two-dimensional hexagonal Fermi-Pasta-Ulam lattice, *J. Phys. A: Math. Theor.* **40**, 1239 (2007).
- [93] V. A. Kuzkin and A. M. Krivtsov, An analytical description of transient thermal processes in harmonic crystals, *Phys. Solid State* **59**, 1051 (2017).
- [94] D. S. Ryabov, G. M. Chechin, A. Upadhyaya, E. A. Korznikova, V. I. Dubinko, and S. V. Dmitriev, Delocalized nonlinear vibrational modes of triangular lattices, *Nonlinear Dyn.* **102**, 2793 (2020).
- [95] G. M. Chechin, D. S. Ryabov, and K. G. Zhukov, Stability of low-dimensional bushes of vibrational modes in the Fermi-Pasta-Ulam chains, *Physica D* **203**, 121 (2005).
- [96] V. P. Sakhnenko and G. M. Chechin, Symmetrical selection rules in nonlinear dynamics of atomic systems, *Phys. Dokl.* **38**, 219 (1993).
- [97] V. P. Sakhnenko and G. M. Chechin, Bushes of modes and normal modes for nonlinear dynamical systems with discrete symmetry, *Phys. Dokl.* **39**, 625 (1994).
- [98] G. M. Chechin and V. P. Sakhnenko, Interactions between

- normal modes in nonlinear dynamical systems with discrete symmetry, Exact results, *Physica D* **117**, 43 (1998).
- [99] G. M. Chechin and D. S. Ryabov, Introduction to the theory of bushes of nonlinear normal modes for studying large-amplitude atomic vibrations in systems with discrete symmetry, *Lett. Mater.* **10**, 523 (2020).
- [100] S. A. Shcherbinin, M. N. Semenova, A. S. Semenov, E. A. Korznikova, G. M. Chechin, and S. V. Dmitriev, Dynamics of a three-component delocalized nonlinear vibrational mode in graphene, *Phys. Solid State* **61**, 2139 (2019).
- [101] G. Chechin, D. Ryabov, and S. Shcherbinin, Nonlinear normal mode interactions in the SF<sub>6</sub> molecule studied with the aid of density functional theory, *Phys. Rev. E* **92**, 012907 (2015).
- [102] G. M. Chechin and S. A. Shcherbinin, Delocalized periodic vibrations in nonlinear LC and LCR electrical chains, *Commun. Nonlinear Sci.* **22**, 244 (2015).
- [103] A. A. Kistanov, R. T. Murzaev, S. V. Dmitriev, V. I. Dubinko, and V. V. Khizhnyakov, Moving discrete breathers in a monoatomic two-dimensional crystal, *JETP Lett.* **99**, 353 (2014).
- [104] E. A. Korznikova, S. Yu. Fomin, E. G. Soboleva, and S. V. Dmitriev, Highly symmetric discrete breather in a two-dimensional Morse crystal, *JETP Lett.* **103**, 277 (2016).
- [105] G. Chechin, D. Ryabov, and S. Shcherbinin, Large-amplitude periodic atomic vibrations in diamond, *J. Micromechanics Mol. Phys.* **3**, 1850002 (2018).
- [106] K. A. Krylova, I. P. Lobzenko, A. S. Semenov, A. A. Kudreyko, and S. V. Dmitriev, Spherically localized discrete breathers in bcc metals V and Nb, *Comp. Mater. Sci.* **180**, 109695 (2020).
- [107] G. M. Chechin, D. S. Ryabov, and S. A. Shcherbinin, Large-amplitude in-plane atomic vibrations in strained graphene monolayer: Bushes of nonlinear normal modes, *Lett. Mater.* **7**, 367 (2017).
- [108] E. A. Korznikova, S. A. Shcherbinin, D. S. Ryabov, G. M. Chechin, E. G. Ekomasov, E. Barani, K. Zhou, and S. V. Dmitriev, Delocalized nonlinear vibrational modes in graphene: Second harmonic generation and negative pressure, *Phys. Status Solidi B* **256**, 1800061 (2019).
- [109] D. U. Abdullina, M. N. Semenova, A. S. Semenov, E. A. Korznikova, and S. V. Dmitriev, Stability of delocalized nonlinear vibrational modes in graphene lattice, *Eur. Phys. J. B* **92**, 249 (2019).
- [110] I. R. Sunagatova, A. M. Subkhangulova, M. N. Semenova, D. I. Borisov, A. S. Semenov, and S. V. Dmitriev, Properties of one-dimensional nonlinear vibrational modes in triangular lattice with Lennard-Jones interactions, *IOP Conf. Ser.: Mater. Sci. Eng.* **1008**, 012073 (2020).
- [111] Y. Watanabe and S. Izumi, Two-dimensional intrinsic localized mode solutions in hexagonal Fermi-Pasta-Ulam lattice, *J. Phys. Soc. Jpn.* **90**, 014003 (2021).
- [112] N. S. Bakhvalov, *Numerical Methods: Analysis, Algebra, Ordinary Differential Equations* (MIR Publishers, Moscow, 1977).
- [113] A. C. Ugural and S. K. Fenster, *Advanced Strength and Applied Elasticity*, 4th ed. (Prentice Hall, Englewood Cliffs, NJ, 2003).
- [114] A. A. Kistanov, S. V. Dmitriev, A. P. Chetverikov, and M. G. Velarde, Head-on and head-off collisions of discrete breathers in two-dimensional anharmonic crystal lattices, *Eur. Phys. J. B* **87**, 211 (2014).
- [115] J. A. D. Wattis and A. S. M. Alzaidi, Asymptotic analysis of breather modes in a two-dimensional mechanical lattice, *Physica D* **401**, 132207 (2020).